

# PCCP

Accepted Manuscript



This is an *Accepted Manuscript*, which has been through the Royal Society of Chemistry peer review process and has been accepted for publication.

*Accepted Manuscripts* are published online shortly after acceptance, before technical editing, formatting and proof reading. Using this free service, authors can make their results available to the community, in citable form, before we publish the edited article. We will replace this *Accepted Manuscript* with the edited and formatted *Advance Article* as soon as it is available.

You can find more information about *Accepted Manuscripts* in the [Information for Authors](#).

Please note that technical editing may introduce minor changes to the text and/or graphics, which may alter content. The journal's standard [Terms & Conditions](#) and the [Ethical guidelines](#) still apply. In no event shall the Royal Society of Chemistry be held responsible for any errors or omissions in this *Accepted Manuscript* or any consequences arising from the use of any information it contains.

*Phys. Chem. Chem. Phys.*

**Gas Phase Complexes of  $\text{H}_3\text{N}\cdots\text{CuF}$  and  $\text{H}_3\text{N}\cdots\text{CuI}$  Studied by  
Rotational Spectroscopy and Ab Initio Calculations: The Effect of  
X (X = F, Cl, Br, I) in  $\text{OC}\cdots\text{CuX}$  and  $\text{H}_3\text{N}\cdots\text{CuX}$**

Dror M. Bittner,<sup>a</sup> Susanna L. Stephens,<sup>ab</sup> Daniel P. Zaleski,<sup>ac</sup> David P. Tew,<sup>d</sup>

Nicholas R. Walker<sup>\*a</sup> and Anthony C. Legon<sup>\*d</sup>

a. School of Chemistry, Bedson Building, Newcastle University, Newcastle upon Tyne, Tyne and Wear, NE1 7RU, U.K.

b. [Current address: Chemistry Department, 360 Parker Building, University of Manitoba, Winnipeg, MB, R3T 2N2, Canada]

c. [Current address: Argonne National Laboratory, Chemical Sciences & Engineering, 9700 S. Cass Ave., Bldg. 200, Lemont, IL 60439, U.S.A.]

d. School of Chemistry, University of Bristol, Cantock's Close, Bristol, BS8 1TS, U.K.

\*Corresponding author email: [nick.walker@newcastle.ac.uk](mailto:nick.walker@newcastle.ac.uk), [a.c.legon@bristol.ac.uk](mailto:a.c.legon@bristol.ac.uk)

**KEYWORDS:** Rotational spectroscopy, ammonia, copper halide, molecular geometry.

## ABSTRACT

Complexes of  $\text{H}_3\text{N}\cdots\text{CuF}$  and  $\text{H}_3\text{N}\cdots\text{CuI}$  have been synthesised in the gas phase and characterized by microwave spectroscopy. The rotational spectra of 4 isotopologues of  $\text{H}_3\text{N}\cdots\text{CuF}$  and 5 isotopologues of  $\text{H}_3\text{N}\cdots\text{CuI}$  have been measured in the 6.5–18.5 GHz frequency range using a chirped-pulse Fourier transform microwave spectrometer. Each complex is generated from a gas sample containing  $\text{NH}_3$  and a halogen precursor diluted in Ar. Copper is introduced by laser ablation of a solid target prior to supersonic expansion of the sample into the vacuum chamber of the microwave spectrometer. The spectrum of each complex is characteristic of a symmetric rotor and a  $C_{3v}$  geometry in which the N, Cu and X atoms (where X is F or I) lie on the  $C_3^a$  axis. The rotational constant ( $B_0$ ), centrifugal distortion constants ( $D_J$  and  $D_{JK}$ ), nuclear spin-rotation ( $C_{bb}(\text{Cu})=C_{cc}(\text{Cu})$ ) constant (for  $\text{H}_3\text{N}\cdots\text{CuF}$  only) and nuclear quadrupole coupling constants ( $\chi_{aa}(X)$  where  $(X = \text{N}, \text{Cu}, \text{I})$ ) are fitted to the observed transition frequencies. Structural parameters are determined from the measured rotational constants and also calculated *ab initio* at the CCSD(T)(F12\*)/AVQZ level of theory. Force constants describing the interaction between ammonia and each metal halide are determined from  $D_J$  for each complex. Trends in the interaction strengths and geometries of  $\text{B}\cdots\text{CuX}$  ( $\text{B} = \text{NH}_3, \text{CO}$ ) ( $\text{X} = \text{F}, \text{Cl}, \text{Br}, \text{I}$ ) are discussed.

## 1. Introduction

Gerry and co-workers demonstrated that  $B\cdots MX$  complexes, where B is a Lewis base, M is a coinage metal, and X is a halogen atom, can be generated through laser vaporisation of a metal target in the presence of a gas sample undergoing supersonic expansion, then interrogated by microwave spectroscopy.<sup>1</sup> The pure rotational spectra of  $OC\cdots MX$  ( $X=F, Cl, Br$ ) were measured and interpreted to determine the geometries of the complexes. An extensive and systematic study of the rotational spectra of  $B\cdots MX$  complexes, also generated by a combination of laser vaporisation and supersonic expansion, has since been performed. Complexes where the Lewis base is  $H_2$ ,<sup>2, 3</sup>  $N_2$ ,<sup>4</sup>  $CO$ ,<sup>1, 5, 6</sup>  $H_2O$ ,<sup>7</sup>  $H_2S$ ,<sup>8</sup>  $NH_3$ ,<sup>9, 10</sup>  $C_2H_2$ ,<sup>11, 12</sup>  $C_2H_4$ ,<sup>13, 14</sup> or  $c-C_3H_6$ <sup>15</sup> have been reported. Metal-containing ( $B\cdots MX$ ) complexes have also been investigated by *ab initio* methods which have explored the nature of bonding interactions and the influence of the halide on the interaction between the metal and the Lewis base.<sup>16-19</sup>

This work presents analyses of the rotational spectra of  $H_3N\cdots CuI$  and  $H_3N\cdots CuF$ . The structures of the complexes as well as the strengths of interactions between  $NH_3$  and the different  $CuX$  ( $X=F, I$ ) molecules are determined from measured spectroscopic constants and through *ab initio* calculations. Unlike  $H_3N\cdots CuCl$ , for which a crystal structure<sup>20</sup> was known before its observation in the gas phase,  $H_3N\cdots CuI$  and  $H_3N\cdots CuF$  have not been structurally characterised in the condensed phase. The reaction of copper(II) fluoride and copper metal with ammonia has been observed both in gaseous and in anhydrous liquid ammonia.<sup>21</sup> Among the products obtained were copper(I) fluoride and copper(II) fluoride ammine complexes. It has been suggested that copper(I) fluoride ammine complexes may serve as intermediates that allow the isolation of binary copper(I) fluoride which has not yet been characterized in the solid phase. The results of the present work are compared with those of the previously published reports on  $H_3N\cdots CuCl$ <sup>10</sup> and  $OC\cdots CuX$  ( $X=F, Cl, Br, I$ ).<sup>1, 22</sup> Clear trends are identified and described. Legon and co-workers earlier performed systematic studies of hydrogen- and halogen-bonded complexes,  $B\cdots HX$ <sup>23</sup> and  $B\cdots XY$ <sup>24</sup> (where Y is a halogen atom). The present work compares the properties of  $H_3N\cdots MX$  with selected  $H_3N\cdots HX$  and  $H_3N\cdots XY$  complexes that have been characterised previously.

## 2. Experimental and theoretical methods

Broadband microwave spectra were measured using a chirped-pulse Fourier-transform microwave (CP-FTMW) spectrometer fitted with a laser ablation source. Detailed descriptions of the spectrometer and laser ablation source are provided in Ref. 25 and Ref. 26. A gas sample containing ~4.0% NH<sub>3</sub> and ~1.5% SF<sub>6</sub> (when generating H<sub>3</sub>N...CuF) or CF<sub>3</sub>I (when generating H<sub>3</sub>N...CuI) is diluted in argon and prepared at a total pressure of 6 bar. The sample is pulsed (from a General Valve, using pulse length of 960 μs set using Parker-Hannifin Iota One Valve Driver) into the vacuum chamber of the spectrometer and passes over the surface of a copper rod that is ablated by a Nd:YAG laser pulse (λ=532 nm, pulse duration of 10 ns, pulse energy of 20 mJ) before undergoing supersonic expansion. A repetition rate of ~1.05 Hz is employed. The copper rod is continually translated and rotated in order to expose a fresh surface to each laser pulse and to ensure shot-to-shot reproducibility of signal intensities. Isotopically-enriched samples of <sup>15</sup>NH<sub>3</sub> (Sigma-Aldrich, 98% <sup>15</sup>N) and ND<sub>3</sub> (Sigma-Aldrich, 99% D) were used to detect <sup>15</sup>NH<sub>3</sub>- and ND<sub>3</sub>-containing complexes respectively.

The sequence employed to record broadband microwave spectra involves (i) polarization of the sample by a microwave chirp that sweeps from 6.5 to 18.5 GHz within 1 μs and (ii) recording of the free induction decay of the molecular emission over a subsequent period of 20 μs. The sequence of (i) and (ii) is repeated eight times following each gas sample introduction pulse. The free induction decay (FID) of the polarization is digitized using a 25 Gs/s digital oscilloscope after down-mixing against a 19 GHz local oscillator. Frequency domain spectra are obtained through a Fourier transform that uses the high resolution window function (full width at half maximum (FWHM) ~65 Hz) described by Tektronix (details provided as Supplementary Information). The spectra of H<sub>3</sub>N...<sup>63/65</sup>CuF, H<sub>3</sub><sup>15</sup>N...CuF and D<sub>3</sub>N...<sup>63</sup>CuF were averaged for 1,500k, 540k and 2,520k free induction decays (FIDs) respectively prior to being Fourier transformed. The spectra of H<sub>3</sub>N...<sup>63/65</sup>CuI, H<sub>3</sub><sup>15</sup>N...CuI and D<sub>3</sub>N...<sup>63/65</sup>CuI were averaged for 660k, 180k and 540k FIDs respectively prior to being Fourier transformed.

Structure optimizations and counter-poise corrected dissociation energies were calculated using the molpro package<sup>27</sup> at the CCSD(T)(F12\*) level of theory,<sup>28</sup> a coupled-cluster method with single and double excitations, explicit correlation,<sup>29</sup> and a perturbative treatment of triple excitations.<sup>30</sup> Only valence electrons are included in the correlation treatment. A basis set combination consisting of aug-cc-pVQZ on H, N and F atoms and aug-cc-pVQZ-PP on Cu and I atoms was used and will be referred to by AVQZ. ECP-10-MDF<sup>31, 32</sup> and ECP-28-MDF<sup>33, 34</sup> were used on Cu and I respectively to account for scalar relativistic effects. For the density fitting approximation used to accelerate the CCSD(T)(F12\*) calculation, the respective def2-QZVPP basis sets were employed for the MP2<sup>35</sup> and Fock<sup>36</sup> terms. For the complementary auxiliary basis required for the F12 treatment,<sup>37</sup> the def2-TZVPP MP2 density fitting basis sets were used.<sup>38</sup> Force constants were calculated from the second derivative of the energy with respect to the internal coordinates using the GAUSSIAN 09 package<sup>39</sup> at the MP2 level of theory. A basis set combination consisting of aug-cc-pVTZ on H, N and F atoms, aug-cc-pVTZ-PP on Cu and I atoms was used.

### 3. Results

#### 3.1 Spectral analysis and Assignment

Figure 1 displays sections of the broadband spectrum measured when probing a gas sample containing CF<sub>3</sub>I, NH<sub>3</sub> and argon that interacts with the plasma plume produced by ablation of the copper rod. The most intense transitions are observed for CF<sub>3</sub>I<sup>40</sup> while those of NH<sub>3</sub>⋯Ar,<sup>41</sup> CF<sub>3</sub>I⋯NH<sub>3</sub>,<sup>42</sup> IF<sup>43</sup> and CuI<sup>44</sup> are also strong. The spectrum of H<sub>3</sub>N⋯CuI was identified through the analysis of groups of transitions, significantly weaker in intensity than those of the species listed above, which are separated by frequency increments of ~2.2 GHz. Distinctive and extensive hyperfine splittings are present in each  $J' \rightarrow J''$  transition as expected for a complex that contains copper and iodine nuclei (which have  $I = 3/2$  and  $5/2$  respectively). A different range of chemical products was observed, including NH<sub>3</sub>⋯SF<sub>6</sub>,<sup>45</sup> NH<sub>3</sub>⋯Ar<sup>41</sup> and (NH<sub>3</sub>)<sub>2</sub><sup>46</sup> after exchanging the gas sample for another that contains SF<sub>6</sub>, NH<sub>3</sub> and argon. The frequency of the  $J' \rightarrow J'' = 1 \rightarrow 0$  transition of CuF lies above the upper limit of the spectrometer. Consecutive  $J' \rightarrow J''$  transitions of H<sub>3</sub>N⋯CuF, which have lower intensities than those of NH<sub>3</sub>⋯SF<sub>6</sub>, NH<sub>3</sub>⋯Ar and (NH<sub>3</sub>)<sub>2</sub>, were observed at intervals of ~8.0 GHz and

display hyperfine structure arising from the presence of the copper nucleus ( $I=3/2$ ). The  $J' \rightarrow J'' = 1 \rightarrow 0$  and  $2 \rightarrow 1$  transitions of  $\text{H}_3\text{N}\cdots\text{CuF}$  are shown in Figure 2. The spectra observed for each of  $\text{H}_3\text{N}\cdots\text{CuF}$  and  $\text{H}_3\text{N}\cdots\text{CuI}$  contain only  $a$ -type transitions, consistent with the  $C_{3v}$  geometries (Figure 3) anticipated for each of these complexes and previously observed for each of  $\text{H}_3\text{N}\cdots\text{AgCl}^9$  and  $\text{H}_3\text{N}\cdots\text{CuCl}^{10}$ .

**Figure 1.** Top panel. The broadband rotational spectrum (660k FIDs) obtained while using a gas sample containing small concentrations of  $\text{CF}_3\text{I}$  and  $\text{NH}_3$  diluted in argon. a)  $J' \rightarrow J'' = 7 \rightarrow 6$  transitions of  $\text{H}_3\text{N}\cdots^{63}\text{CuI}$ . b)  $J' \rightarrow J'' = 4 \rightarrow 3$  transitions of  $^{63}\text{CuI}$ . c)  $J' \rightarrow J'' = 6 \rightarrow 5$  transitions of  $\text{H}_3\text{N}\cdots\text{ICF}_3$ . d)  $J' \rightarrow J'' = 2 \rightarrow 1$  transition in the  $\Sigma_{0a}$  state of  $\text{NH}_3\cdots\text{Ar}$ .

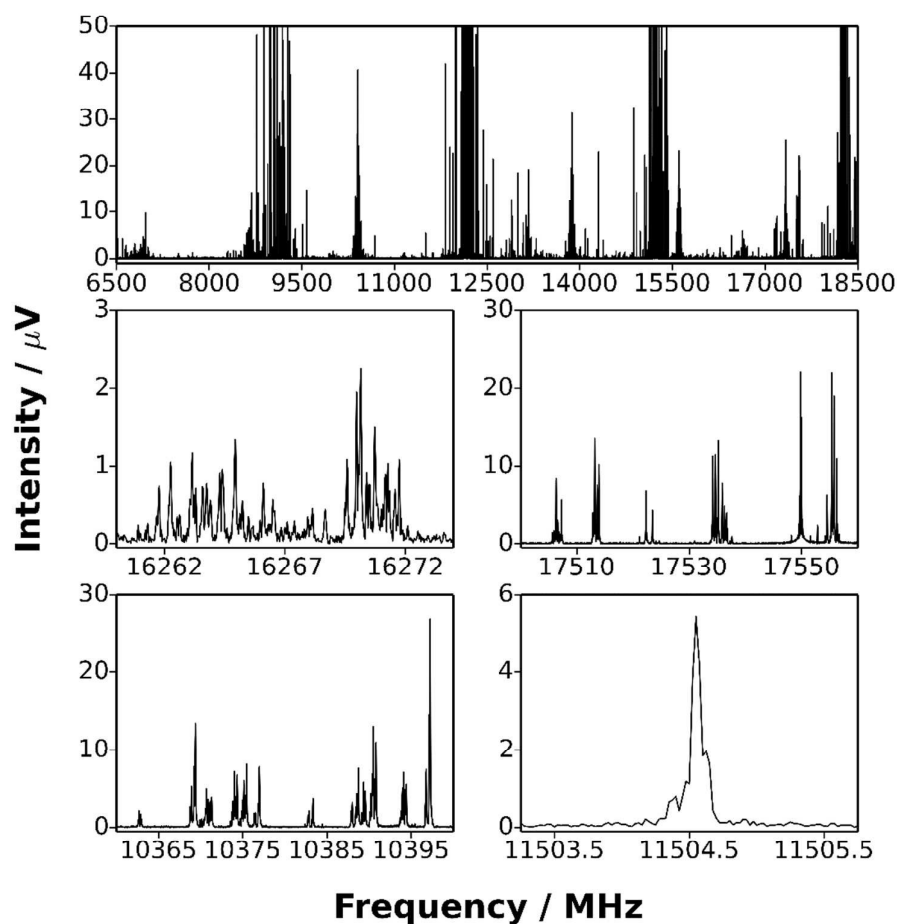


**Figure 2.** Top panel. A section of the broadband spectrum showing  $J' \rightarrow J'' = 1 \rightarrow 0$  transitions of  $\text{H}_3\text{N}\cdots\text{CuF}$  (black trace) and a simulation of the transitions of  $\text{H}_3\text{N}\cdots^{63}\text{CuF}$  and  $\text{H}_3\text{N}\cdots^{65}\text{CuF}$  (red and blue traces respectively). Bottom panel. A section of the broadband spectrum showing  $J' \rightarrow J'' = 2 \rightarrow 1$  transitions of  $\text{H}_3\text{N}\cdots\text{CuF}$  (black trace) and a simulation of the transitions of  $\text{H}_3\text{N}\cdots^{63}\text{CuF}$  and  $\text{H}_3\text{N}\cdots^{65}\text{CuF}$  (red and blue traces respectively).

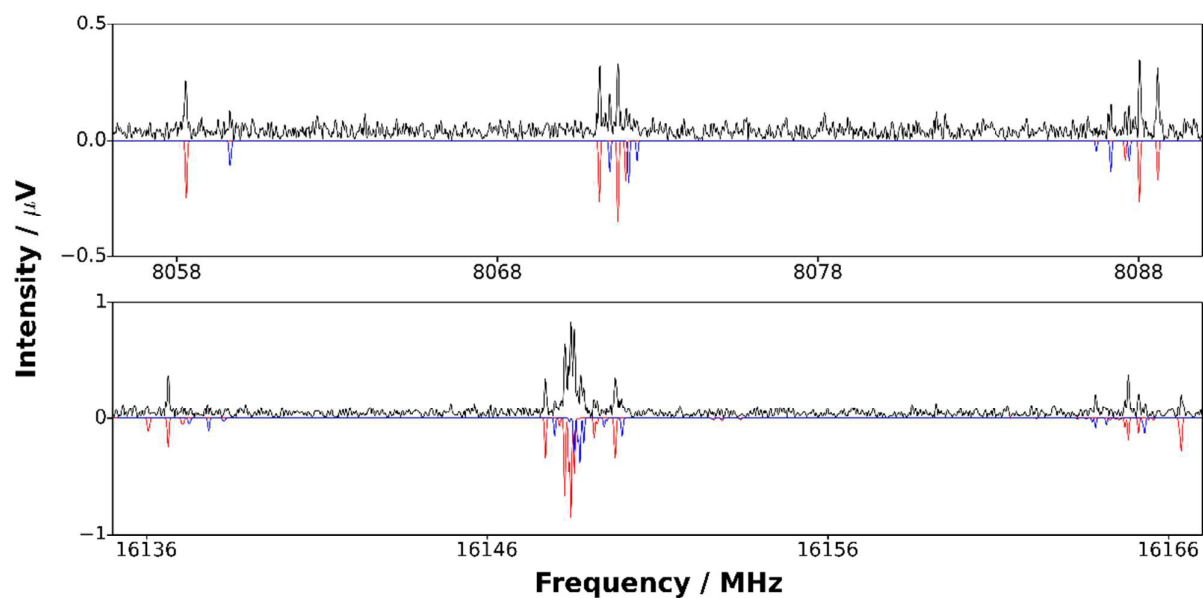
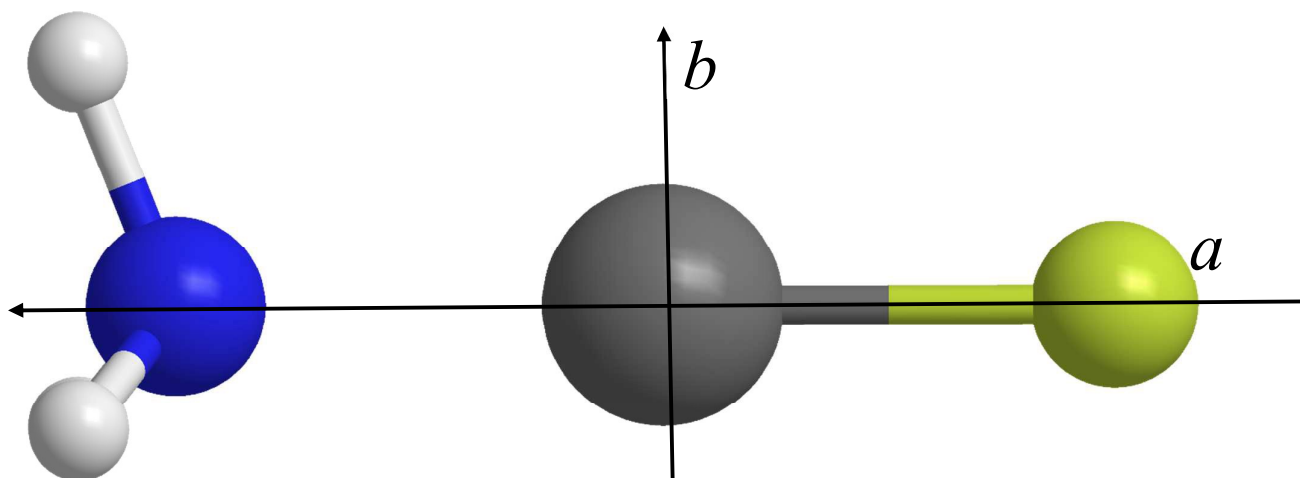


**Figure 3.** The structure of  $\text{H}_3\text{N}\cdots\text{CuF}$ . N, Cu and F are the blue, grey and green spheres respectively. The  $a$  and  $b$  principal axes are shown.





Western's PGOPHER<sup>47</sup> was used to fit parameters in the Hamiltonian shown below to the observed transitions of each complex;

$$H = H_R - \frac{1}{6} \mathbf{Q}(\text{Cu}) : \nabla \mathbf{E}(\text{Cu}) - \frac{1}{6} \mathbf{Q}(\text{I}) : \nabla \mathbf{E}(\text{I}) - \frac{1}{6} \mathbf{Q}(\text{N}) : \nabla \mathbf{E}(\text{N}) + \mathbf{I}_{\text{Cu}} \cdot \mathbf{C}_{\text{Cu}} \cdot \mathbf{J} \quad (1)$$

where  $H_R$  is the Hamiltonian of a semi-rigid, prolate symmetric rotor. The second, third, and fourth terms on the right hand side describe the coupling of the nuclear electric quadrupole moment with the electric field gradient at each of the Cu, I and N nuclei (respectively). The interaction is given by the scalar (or inner) product of the nuclear quadrupole moment dyadic,  $\mathbf{Q}$ , and the dyadic of the electric field gradient arising from extra nuclear charges,  $\nabla \mathbf{E}$ . The nuclear quadrupole coupling constants are denoted by  $\chi_{aa}(X)$  (where  $X$  is Cu, N or I) and can be determined from the nuclear quadrupole hyperfine structure. The last term describes the magnetic hyperfine interaction between the nuclear magnetic moment of Cu and the effective magnetic field generated by the rotation of the molecular framework. An attempt to fit [ $C_{bb}(\text{Cu})=C_{cc}(\text{Cu})$ ] for  $\text{H}_3^{14}\text{N}\cdots^{63/65}\text{CuI}$  yielded a result with uncertainty similar to the value of the parameter. It was therefore not included in the parameter set used in the final fits. The coupling scheme used for  $\text{H}_3^{14}\text{N}\cdots^{63/65}\text{CuI}$  and  $\text{D}_3^{14}\text{N}\cdots^{63}\text{CuI}$  is  $F_1=J+I_I$ ,  $F_2=F_1+I_{\text{Cu}}$  and  $F=F_2+I_{\text{N}}$ . For  $\text{H}_3^{14}\text{N}\cdots^{63/65}\text{CuF}$  and  $\text{D}_3^{14}\text{N}\cdots^{63}\text{CuF}$ , the coupling scheme is  $F_1=J+I_{\text{Cu}}$  and  $F=F_1+I_{\text{N}}$ . Given that  $I_{\text{N}}=1/2$  for  $^{15}\text{N}$  and that the described experiments do not resolve any hyperfine splittings introduced by the  $^{15}\text{N}$  nucleus, the term of Eqn.(1) that applies to the nitrogen atom is omitted when fitting the spectra of isotopologues containing  $^{15}\text{N}$ . Hyperfine splittings introduced by the hydrogen and fluorine nuclei were also not resolved by the present experiments. In every case, the  $A_0$  rotational constant is fixed to the value of  $C_0$  for free ammonia for the purpose of simulating intensities. The results of spectroscopic fits are provided in Tables 1 and 2 for  $\text{H}_3\text{N}\cdots\text{CuF}$  and  $\text{H}_3\text{N}\cdots\text{CuI}$  respectively.

**Table 1.** Determined spectroscopic constants of 4 isotopologues of  $\text{H}_3\text{N}\cdots\text{CuF}$

|   | $\text{H}_3\text{N}\cdots^{63}\text{CuF}$ | $\text{H}_3\text{N}\cdots^{65}\text{CuF}$ | $\text{D}_3\text{N}\cdots^{63}\text{CuF}$ | $\text{H}_3^{15}\text{N}\cdots^{63}\text{CuF}$ |
|---|---|---|---|--|
| $B_0$ / MHz                                     | 4037.4554(19) <sup>a</sup>                | 4037.513(10)                              | 3570.3874(16)                             | 3926.6944(36)                                  |
| $D_J$ / kHz                                     | 1.20(25)                                  | 2.9(13)                                   | [1.20] <sup>b</sup>                       | 1.04(48)                                       |
| $\chi_{aa}(\text{Cu})$ / MHz                    | 66.196(12)                                | 61.183(61)                                | 66.441(68)                                | 66.212(21)                                     |
| $\chi_{aa}(\text{N})$ / MHz                     | -2.717(15)                                | -2.787(90)                                | -2.776(41)                                | -  |
| [ $C_{bb}(\text{Cu})=C_{cc}(\text{Cu})$ ] / kHz | 18.9(12)                                  | [20.2] <sup>c</sup>                       | 21.7(54)                                  | 17.3(23)                                       |
| $N^d$   | 18  | 8   | 8   | 7  |
| $\sigma_{r.m.s.}^d$ / kHz                       | 7.4                                       | 23.8                                      | 15.8                                      | 9.1  |

<sup>a</sup> Numbers in parentheses are one standard deviation in units of the last significant figure.

<sup>b</sup> Value in square brackets is fixed to the result for H<sub>3</sub>N...<sup>63</sup>CuF.

<sup>c</sup> The value in square brackets has been determined by scaling  $C_{bb}=C_{cc}$  for H<sub>3</sub>N...<sup>63</sup>CuF by the ratio of the magnetic moments of the <sup>65</sup>Cu and <sup>63</sup>Cu nuclei.

<sup>d</sup>  $N$  is the number of fitted transitions,  $\sigma_{r.m.s.}$  denotes the r.m.s. deviation of the fit.

**Table 2.** Determined spectroscopic constants of 5 isotopologues of H<sub>3</sub>N...CuI.

|                              | H <sub>3</sub> N... <sup>63</sup> CuI | H <sub>3</sub> N... <sup>65</sup> CuI | D <sub>3</sub> N... <sup>63</sup> CuI | D <sub>3</sub> N... <sup>65</sup> CuI | H <sub>3</sub> <sup>15</sup> N... <sup>63</sup> CuI |
|------------------------------|---------------------------------------|---------------------------------------|---------------------------------------|---------------------------------------|---|
| $B_0$ / MHz                  | 1162.03613(67) <sup>a</sup>           | 1153.4533(19)                         | 1064.91348(73)                        | 1058.27044(50)                        | 1135.26715(70)                                      |
| $D_J$ / kHz                  | 0.1289(73)                            | 0.097(17)                             | 0.0907(72)                            | [0.097] <sup>b</sup>                  | 0.1048(63)  |
| $D_{JK}$ / kHz               | 12.96(26)                             | 9.73(80)                              | 9.66(54)                              | 10.91(95)                             | 14.15(47)   |
| $\chi_{aa}(\text{Cu})$ / MHz | 62.943(95)                            | 58.70(44)                             | 63.75(17)                             | 58.99(41)                             | 62.55(29)   |
| $\chi_{aa}(\text{N})$ / MHz  | -2.28(11)                             | -2.18(41)                             | -2.59(19)                             | -2.82(18)                             | -   |
| $\chi_{aa}(\text{I})$ / MHz  | -613.99(28)                           | -613.62(77)                           | -612.86(49)                           | -614.32(77)                           | -614.25(43)   |
| $N^c$                        | 71                                    | 35                                    | 46                                    | 14                                    | 32  |
| $\sigma_{r.m.s.}^d$ / kHz    | 13.2                                  | 20.3                                  | 21.0                                  | 14.6                                  | 12.2  |

<sup>a</sup> Numbers in parentheses are one standard deviation in units of the last significant figure.

<sup>b</sup> Numbers in square brackets have been fixed.

<sup>c</sup>  $N$  is the number of fitted transitions.

<sup>d</sup>  $\sigma_{r.m.s.}$  denotes the r.m.s. deviation of the fit.

All spectra were measured using a copper sample containing <sup>63</sup>Cu and <sup>65</sup>Cu isotopes in their natural abundances. The intensities of the spectra of all isotopologues are consistent with the natural fractional abundances of <sup>63</sup>Cu and <sup>65</sup>Cu which are 69% and 31% respectively. Isotopically-enriched samples were used to allow measurement and assignment of the spectra of D<sub>3</sub>N...<sup>63/65</sup>CuI, H<sub>3</sub><sup>15</sup>N...<sup>63</sup>CuI, D<sub>3</sub>N...<sup>63</sup>CuF and H<sub>3</sub><sup>15</sup>N...<sup>63</sup>CuF. Given that only one isotope of each of fluorine and iodine is available, isotopic substitution was not possible at the halogen atom. Confirmation that the molecular carriers of the observed spectra contain copper was obtained through comparison of the nuclear quadrupole coupling constants,  $\chi_{aa}(\text{Cu})=eQq_{aa}(\text{Cu})$ , for the various isotopologues. This nuclear quadrupole coupling constant provides a measure of the strength of the coupling of the electric field gradient ( $q_{aa}$ ) at the Cu nucleus along the axis  $a$  with the ‘conventional’ nuclear electric quadrupole moment  $eQ$ , defined as  $eQ = \langle I, I | Q_{zz} | I, I \rangle$ . Note that both the dyadic  $\mathbf{Q}$  and its element  $Q_{zz}$  contain the nuclear charge density while the constant  $Q$  does not; hence multiplication by the charge of a proton  $e$  on the left-hand side of the definition. For any given isotopologue, the electric field gradient is invariant to isotopic exchange (to a very good first approximation) even in the zero-point state so the ratio of the values of  $\chi_{aa}(\text{Cu})$  in B...<sup>63</sup>CuX and  $\chi_{aa}(\text{Cu})$  in B...<sup>65</sup>CuX should be

equal to the ratio of the nuclear electric quadrupole moments of  $^{63}\text{Cu}$  and  $^{65}\text{Cu}$ . This condition is satisfied with the required level of precision for each pair of isotopologues for which the ratio can be calculated. The fitted rotational constant of  $\text{H}_3\text{N}\cdots^{63}\text{CuF}$  is slightly smaller than that of  $\text{H}_3\text{N}\cdots^{65}\text{CuF}$ . This implies that the Cu atom is sufficiently close to the centre of mass of this complex that any decrease in rotational constant (which would be required under the assumption of a rigid molecular framework, if Cu is not exactly at the centre of mass) is compensated by zero point effects. The rotational constant of  $\text{H}_3\text{N}\cdots^{63}\text{CuI}$  is greater than that of  $\text{H}_3\text{N}\cdots^{65}\text{CuI}$  by about 10 MHz. For  $\text{H}_3\text{N}\cdots^{63}\text{CuI}$ , comparing the intensities of transitions having  $K=1$  with those having  $K=0$ , the former are observed to be significantly more intense than would be expected at a rotational temperature of 2 K. This enhanced population of  $K=1$  states has been discussed previously<sup>10</sup> and is explained by a reduced efficiency of collisional relaxation when the symmetry of a complex allows for hydrogen atoms to be exchanged by a  $C_3$  rotation about the inertial  $a$  axis.  $K=0$  and  $K=1, 2$  transitions belong to different symmetry species with relaxation taking place only within the two stacks, such that  $K=0$  and  $K=1$  transitions become equal in intensity because  $K=0$  transitions have twice the statistical weight of each of  $K=1, 2$ . This is consistent with the ratio of the observed intensities of  $K=0$  and  $K=1$  transitions of  $\text{H}_3\text{N}\cdots\text{CuI}$ . Transitions having  $K=2$  were not observed for either  $\text{H}_3\text{N}\cdots\text{CuF}$  or  $\text{H}_3\text{N}\cdots\text{CuI}$ . Transitions having  $K=1$  were not observed for  $\text{H}_3\text{N}\cdots\text{CuF}$  for which only  $J' \rightarrow J'' = 1 \rightarrow 0$  and  $2 \rightarrow 1$  transitions are within the frequency range probed by the spectrometer.

### 3.2 Molecular Geometry

By analogy with the geometries previously determined for the  $\text{H}_3\text{N}\cdots\text{AgCl}$ <sup>9</sup> and  $\text{H}_3\text{N}\cdots\text{CuCl}$ <sup>10</sup> complexes, it will initially be assumed that  $\text{H}_3\text{N}\cdots\text{CuX}$  ( $X=\text{F}, \text{I}$ ) adopt a  $C_{3v}$  symmetry in which N, Cu and X are located on the inertial  $a$  axis while interconnected in the geometry shown in Figure 3. This assumption is consistent with the observations of  $a$ -type transitions and of a copper atom positioned close to the centre of mass in each of  $\text{H}_3\text{N}\cdots\text{CuF}$  and  $\text{H}_3\text{N}\cdots\text{CuI}$ . From this starting point, effective ground state ( $r_0$ ) and substitution ( $r_s$ ) geometries will be determined by fitting parameters in the model

geometry (Figure 3) to the experimentally-measured rotational constants. *Ab initio* calculations have been performed to establish equilibrium ( $r_e$ ) geometries and other molecular properties.

The STRFIT<sup>48</sup> program is used to fit the  $r_0$  geometries. The experimental results do not allow independent determination of the N–H bond length,  $r(\text{N–H})$ , and the angle defining the positions of the hydrogen atoms,  $\angle(\text{H–N–Cu})$ . For this reason,  $r(\text{N–H})$  is held fixed while the  $r(\text{Cu–X})$ ,  $r(\text{Cu–N})$  and  $\angle(\text{H–N–Cu})$  structural parameters are fitted. The assumed values of  $r(\text{N–H})$  in the  $r_0$  geometries of  $\text{H}_3\text{N}\cdots\text{CuF}$  and  $\text{H}_3\text{N}\cdots\text{CuI}$  are established by; 1) calculating the difference between the  $r_0$  value of  $r(\text{N–H})$  in isolated  $\text{NH}_3$  and the  $r_e$  value of the same parameter calculated at the CCSD(T)/AVQZ level; 2) adding the result of (1) to the  $r_e$  value calculated for  $r(\text{N–H})$  in each of  $\text{H}_3\text{N}\cdots\text{CuF}$  and  $\text{H}_3\text{N}\cdots\text{CuI}$  respectively. Large zero point changes occur in isolated  $\text{NH}_3$  upon substitution of hydrogen atoms for deuterium. A shrinkage of 0.0011 Å in  $r(\text{N–H})$  and an enlargement of 0.04 degrees in  $\angle(\text{H–N–Cu})$  are observed. These changes are assumed to occur in  $\text{H}_3\text{N}\cdots\text{CuF}$  and  $\text{H}_3\text{N}\cdots\text{CuI}$  and are accounted for when fitting structural parameters. Fixing the  $r(\text{N–H})$  distance as described above allows  $r(\text{Cu–X})$ ,  $r(\text{Cu–N})$  and  $\angle(\text{H–N–Cu})$  to be determined with reasonable accuracy. Given that no isotopic substitution is available at either halogen atom, the uncertainties listed in Table 3 will be underestimated but the results agree satisfactorily with the results of the *ab initio* calculations.

The  $a$ -axis coordinates of Cu and N can also be determined by a ( $r_s$ ) substitution method.<sup>49</sup> The equation shown below is appropriate for an atom located on the symmetry axis of a symmetric rotor;

$$|a| = \sqrt{\frac{\Delta I_b}{\mu}} \quad (2)$$

$\Delta I_b$  is the change in the moment of inertia about the  $b$  inertial axis upon substitution,  $\mu$  is the reduced mass for the isotopic substitution and is given by  $\frac{\Delta m M}{\Delta m + M}$  where  $M$  is the mass of the isotopologue selected as parent and  $\Delta m$  is the change in mass upon substitution. The signs assigned to coordinates are those yielding bond lengths consistent with the *ab initio* calculations within acceptable precision limits.

When using eq (2) the  $a$  coordinate is defined with respect to the principal axis system of the parent isotopologue and  $\angle(\text{H-N-Cu})$  and  $r(\text{N-H})$  cannot be independently determined for either  $\text{H}_3\text{N}\cdots\text{CuF}$  or  $\text{H}_3\text{N}\cdots\text{CuI}$ . The scaling procedure applied earlier to fix  $r(\text{N-H})$  when fitting an  $r_0$  geometry is now used to fix an  $r_s$  value. In this case, the difference between the  $r_s$  and  $r_e$  values of  $r(\text{N-H})$  in free  $\text{NH}_3$  is added to the  $r_e$  value calculated for  $r(\text{N-H})$  in  $\text{H}_3\text{N}\cdots\text{CuX}$  to establish the value of  $r(\text{N-H})$  in the  $r_s$  geometry. Thus, a value of  $\angle(\text{H-N-Cu})$  is determined using the equation provided in ref 50. The uncertainties of  $r_s$  coordinates are calculated using  $\delta a = 0.0015/|a|$  as recommended by Costain.<sup>51</sup> All structural parameters and nuclear coordinates are provided in table 3 alongside those of  $\text{H}_3\text{N}\cdots\text{CuCl}$ . The lack of an isotopic substitution at the halogen atom prevents the determination of an  $r_s$  coordinate for the halogen atom.  $r_s$  coordinates determined from Kraitchman's equations<sup>52</sup> are typically closer to  $r_e$  structural parameters than  $r_0$  values owing to partial cancellation of zero point effects when  $r_s$  coordinates are calculated.<sup>53</sup> From table 3 it can be seen that  $r(\text{N-Cu})$  increases with increasing mass of the halogen atom of  $\text{H}_3\text{N}\cdots\text{CuX}$ . The value of  $\angle(\text{H-N-Cu})$  is essentially independent of the halogen atom.

**Table 3.**  $r_s$ ,  $r_0$  and ab initio  $r_e$  structures and the corresponding principal axis coordinates of  $\text{H}_3\text{N}\cdots\text{CuF}$  and  $\text{H}_3\text{N}\cdots\text{CuI}$ .

|                                | $r_0$                            |                                  | $r_s$                            |                                  | $r_e$                            |                                  |
|--------------------------------|----------------------------------|----------------------------------|----------------------------------|----------------------------------|----------------------------------|----------------------------------|
|                                | $\text{H}_3\text{N}$<br>⋮<br>CuF | $\text{H}_3\text{N}$<br>⋮<br>CuI | $\text{H}_3\text{N}$<br>⋮<br>CuF | $\text{H}_3\text{N}$<br>⋮<br>CuI | $\text{H}_3\text{N}$<br>⋮<br>CuF | $\text{H}_3\text{N}$<br>⋮<br>CuI |
| $r(\text{Cu-X})/\text{\AA}$    | 1.74919(55) <sup>a</sup>         | 2.35525(46)                      | -                                | -                                | 1.7372                           | 2.3574                           |
| $r(\text{Cu-N})/\text{\AA}$    | 1.89276(61)                      | 1.9357(13)                       | 1.89(5)                          | 1.9361(13)                       | 1.8804                           | 1.9226                           |
| $r(\text{H-N})/\text{\AA}$     | [1.0187] <sup>b</sup>            | [1.0185]                         | [1.0180]                         | [1.0178]                         | 1.0145                           | 1.0143                           |
| $\angle(\text{H-N-Cu})/^\circ$ | 111.462(26)                      | 111.430(54)                      | 111.500(50)                      | 111.535(30)                      | 111.746                          | 111.811                          |
| $a_{\text{Cu}}/\text{\AA}$     | -0.00124(20)                     | 1.28011(37)                      | 0.00(5) <sup>c</sup>             | 1.27874(121)                     | 0.0014945                        | 1.2825                           |
| $a_{\text{X}}/\text{\AA}$      | -1.75043(35)                     | -1.07511(9)                      | -                                | -                                | -1.7387                          | -1.0750                          |
| $a_{\text{N}}/\text{\AA}$      | 1.89152(41)                      | 3.21585(88)                      | 1.89128(79)                      | 3.21480(47)                      | 1.8789                           | 3.2051                           |
| $a_{\text{H}}/\text{\AA}$      | 2.26426(12)                      | 3.58797(26)                      | -                                | -                                | 2.2548                           | 3.5819                           |
| $b_{\text{H}}/\text{\AA}$      | 0.94806(17)                      | 0.94809(34)                      | -                                | -                                | 0.94230                          | 0.94170                          |

<sup>a</sup> Numbers in parentheses are one standard deviation in units of the last significant figure.

<sup>b</sup> Numbers in square brackets have been fixed at values determined as described under "Molecular Geometry".

<sup>c</sup> An imaginary number was obtained as the Kraitchman coordinate.

### 3.3 Interaction Strength and Ionicity

The strength of the interaction between  $\text{NH}_3$  and  $\text{CuX}$  can be assessed with reference to the dissociation energy for the  $\text{H}_3\text{N}\cdots\text{CuX} \rightarrow \text{NH}_3 + \text{CuX}$  reaction and also the force constant of the  $\text{N}\cdots\text{Cu}$  bond. *Ab initio* calculations of both these quantities have been performed. As shown in Table 4, the dissociation energy of  $\text{H}_3\text{N}\cdots\text{CuX}$  decreases with increasing mass of the halogen atom with the highest result being  $197.0 \text{ kJ mol}^{-1}$  for the  $\text{H}_3\text{N}\cdots\text{CuF}$  complex.

The results of the *ab initio* calculations of the force constants,  $k_\sigma$ , follow the same trend with  $k_\sigma(\text{N}\cdots\text{Cu})$  of  $\text{H}_3\text{N}\cdots\text{CuF}$  found to be  $242 \text{ N m}^{-1}$ . The *ab initio* results for the  $k_\sigma(\text{N}\cdots\text{Cu})$  can be compared with others determined from the experimental data as shown in table 4. The experimentally-determined force constants are calculated by applying a model<sup>54</sup> which accounts for contributions to the centrifugal distortion constants from both the  $\text{Cu-X}$  and  $\text{N}\cdots\text{Cu}$  bonds. The force constants appropriate to the  $\text{Cu-X}$  and  $\text{N}\cdots\text{Cu}$  bonds are denoted by  $F_{11}$  and  $F_{22}$  respectively in Eq 3;

$$hD_J = \frac{1}{2} \left\{ \frac{\hbar^4}{I_{bb}^4} \right\} \{ (m_1 a_1)^2 (F^{-1})_{11} + (m_1 a_1 + m_2 a_2)^2 (F^{-1})_{22} \} \quad (3)$$

where  $m_1$  and  $m_2$  are the masses of the halogen and copper atoms respectively. The principal axis coordinates of the halogen and copper atoms are  $a_1$  and  $a_2$  respectively. This model allows the calculation of either  $F_{11}$  or  $F_{22}$  provided the other is known. Even where neither parameter is accurately known, a good estimate of one will allow an approximate value and uncertainty limits to be assigned to the other.

For each of  $\text{H}_3\text{N}\cdots\text{CuF}$ ,  $\text{H}_3\text{N}\cdots\text{CuCl}$  and  $\text{H}_3\text{N}\cdots\text{CuI}$ , it can initially be assumed that  $F_{11}$  is equal to  $k_\sigma$  of the appropriate, isolated metal halide diatomic.<sup>44, 55, 56</sup> The  $r_0$  coordinates and moments of inertia ( $I_{bb}$ ) calculated from the ground state rotational constants ( $B_0$ ) of the various complexes are then used to determine the  $F_{22}$  values. In the limit of a rigid  $\text{Cu-X}$  bond,  $F_{11}$  tends to infinity and  $F_{22}$  approaches an asymptotic value. Where  $F_{11} \gg F_{22}$ , any change in the assumed value of  $F_{11}$  induces only a very small change in the determined value of  $F_{22}$ . As shown in Figure 4, the assumption that the various  $F_{11}$  are reasonably approximated by  $k_\sigma$  for the isolated metal halides ( $k_\sigma(\text{Cu-F}) = 333 \text{ N m}^{-1}$ ;  $k_\sigma(\text{Cu-I}) = 172 \text{ N m}^{-1}$ ), implies that the bond between the metal and halogen atoms is significantly more rigid than that between the metal and the nitrogen atoms, in each of  $\text{H}_3\text{N}\cdots\text{CuF}$  and  $\text{H}_3\text{N}\cdots\text{CuI}$ .

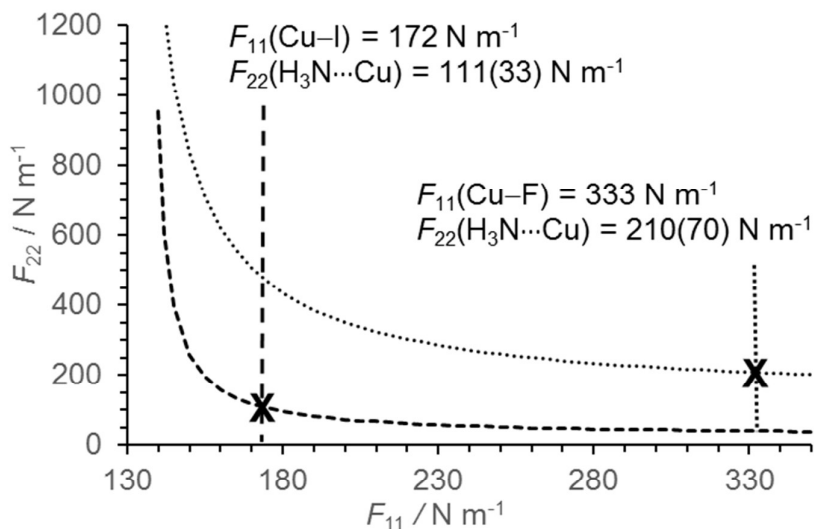


**Figure 4** – Plot to illustrate the variation of  $F_{22}$  as a function of the assumed value of  $F_{11}$  for each of  $\text{H}_3\text{N}\cdots\text{CuF}$  and  $\text{H}_3\text{N}\cdots\text{CuI}$ . The values of  $k_\sigma$  for the isolated  $\text{CuF}$  and  $\text{CuI}$  molecules, assumed equal to  $F_{11}$  in the respective  $\text{H}_3\text{N}\cdots\text{CuF}$  and  $\text{H}_3\text{N}\cdots\text{CuI}$  complexes, are marked with a cross (X).

After propagating the uncertainty in the measured value of  $D_J$ , the assumption that  $F_{11}$  of  $\text{H}_3\text{N}\cdots\text{CuI} = 172 \pm 5 \text{ N m}^{-1}$  implies  $F_{22} = 111(33) \text{ N m}^{-1}$  for  $\text{H}_3\text{N}\cdots\text{CuI}$  where the dominant contribution is the uncertainty in  $D_J$ . An assumed value of  $F_{11}$  for  $\text{H}_3\text{N}\cdots\text{CuF}$  of  $333 \pm 10 \text{ N m}^{-1}$  would imply that  $F_{22}$  falls within a very narrow range between 202 and 210  $\text{N m}^{-1}$ . However, the uncertainty in the measured value of  $D_J$  again makes the dominant contribution and  $F_{22} = 210(70) \text{ N m}^{-1}$  after propagation of the uncertainty in  $D_J$ . The level of agreement between the experimentally-determined results and those calculated *ab initio* is closest for  $\text{H}_3\text{N}\cdots\text{CuF}$  and  $\text{H}_3\text{N}\cdots\text{CuCl}$  which possess the most rigid MX bonds. It is apparent from both the force constants and the dissociation energies that the strengths of  $\text{N}\cdots\text{Cu}$  bonds formed between  $\text{NH}_3$  and MX are in the order  $\text{H}_3\text{N}\cdots\text{CuF} > \text{H}_3\text{N}\cdots\text{CuCl} > \text{H}_3\text{N}\cdots\text{CuI}$ .

Two types of hyperfine interaction have been included in the Hamiltonian. These are the nuclear quadrupole coupling and nuclear spin-rotation interactions. The former allows the determination of the nuclear quadrupole coupling constant,  $eQq(X)$ , for  $X = {}^{14}\text{N}$ ,  ${}^{63/65}\text{Cu}$  and I as appropriate for each isotopologue. The term  $q = \frac{\partial^2 V}{\partial a^2}$  in  $eQq(X)$  represents the electric field gradient with respect to the symmetry axis at atom X. Applying the Townes-Dailey model<sup>57, 58</sup> to interpret the

$eQq(I)$  value of  $\text{H}_3\text{N}\cdots\text{CuI}$ , the ionicity ( $i_c$ ) of the Cu–I bond is calculated to be 0.73 from  $i_c = 1 + \frac{\chi_{aa}(I)}{eQq_{(5,1,0)}(I)}$ , where  $eQq_{(5,1,0)}(I)$  is the coupling constant that would result from the presence of an unpaired electron in the  $5p_z$  orbital of the isolated atom and has a value of 2292.71 MHz.<sup>59</sup> The Townes-Dailey model cannot be readily applied to the analysis of  $eQq$  values of Cu and N.

**Table 4.** Experimental and *ab initio* calculated force constants  $k_\sigma$ , and *ab initio* calculated dissociation energies.

|                                       | $F_{22} = k_\sigma$ (exp.) / [ $\text{N m}^{-1}$ ] | $k_\sigma(\text{MP2/AVTZ})$ / [ $\text{N m}^{-1}$ ] | $D_e(\text{CCSD(T)}(\text{F12*})/\text{AVQZ})$ / [ $\text{kJ mol}^{-1}$ ] |
|---------------------------------------|--|---|---|
| $\text{H}_3\text{N}\cdots\text{CuF}$  | 210(70) <sup>a</sup>                               | 242   | 197   |
| $\text{H}_3\text{N}\cdots\text{CuCl}$ | 170(60) <sup>b</sup>                               | 219   | 183   |
| $\text{H}_3\text{N}\cdots\text{CuI}$  | 111(33) <sup>c</sup>                               | 201   | 168   |

<sup>a</sup> Determined from  $D_J$  of the  $\text{H}_3\text{N}\cdots^{63}\text{CuF}$  isotopologue.

<sup>b</sup> Determined from  $D_J$  of the  $\text{D}_3\text{N}\cdots^{63}\text{Cu}^{35}\text{Cl}$  isotopologue.

<sup>c</sup> Determined from  $D_J$  of the  $\text{H}_3\text{N}\cdots^{63}\text{CuI}$  isotopologue.

#### 4. Conclusions

The spectra of  $\text{H}_3\text{N}\cdots\text{CuF}$  and  $\text{H}_3\text{N}\cdots\text{CuI}$  are each consistent with the  $C_{3v}$  geometry illustrated in Figure 3. Quantitative details of the geometries and measured nuclear quadrupole coupling constants of the  $\text{H}_3\text{N}\cdots\text{CuX}$  series are compared with results from other  $\text{B}\cdots\text{CuX}$  in Table 5. The  $r(\text{Cu-N})$  distances determined for  $\text{H}_3\text{N}\cdots\text{CuF}$  and  $\text{H}_3\text{N}\cdots\text{CuI}$  are consistent with expectations following the earlier study of  $\text{H}_3\text{N}\cdots\text{CuCl}$  and also with the trend established for  $\text{OC}\cdots\text{CuX}$ .  $r(\text{Cu-N})$  lengthens on substituting a lighter by a heavier halogen atom and is longer in  $\text{H}_3\text{N}\cdots\text{CuI}$  than in  $\text{H}_3\text{N}\cdots\text{CuF}$  by 0.043(2) Å. A very similar difference is observed between  $r(\text{Cu-C})$  in  $\text{OC}\cdots\text{CuF}$  and the same parameter in  $\text{OC}\cdots\text{CuI}$ . The trend observed earlier for the  $\text{Ar}\cdots\text{CuX}^{60}$  series involved greater incremental changes on substitution of the halogen atom.  $r(\text{Cu-Ar})$  in  $\text{Ar}\cdots\text{CuF}$  is 0.077(3) Å shorter than the same parameter in  $\text{Ar}\cdots\text{CuBr}$ . The attachment of an isolated  $\text{CuX}$  species to either CO or  $\text{NH}_3$  to form  $\text{B}\cdots\text{CuX}$  causes a change in  $r(\text{Cu-X})$ . The Cu–F bonds of  $\text{H}_3\text{N}\cdots\text{CuF}$  and  $\text{OC}\cdots\text{CuF}$  shrink slightly on formation of these complexes from the isolated  $\text{NH}_3/\text{CO}$  and  $\text{CuX}$  sub-units. In contrast,  $r(\text{Cu-X})$  in the analogous  $\text{B}\cdots\text{CuCl}$ ,  $\text{B}\cdots\text{CuBr}$  and  $\text{B}\cdots\text{CuI}$  species extend slightly on



complex formation. The difference between  $r(\text{Cu}-\text{X})$  in  $\text{B}\cdots\text{CuX}$  and in the corresponding  $\text{CuX}$  diatomic is denoted by  $\Delta r$  in Table 5 for  $\text{H}_3\text{N}\cdots\text{CuX}$  and  $\text{OC}\cdots\text{CuX}$ . For both  $\text{B}=\text{CO}$  and  $\text{B}=\text{NH}_3$ ,  $\Delta r$  is greatest for the iodide. Recent works have described significant changes in the geometry of  $\text{C}_2\text{H}_2$  when it attaches to  $\text{MX}$  to form a T-shaped  $\text{C}_2\text{H}_2\cdots\text{MX}$  complex. Much smaller changes in the bond length of carbon monoxide were identified where  $\text{OC}\cdots\text{CuX}$  and  $\text{OC}\cdots\text{AgX}$  form from their constituent sub-units. At the level of precision of the present experiments and a previous work, the bond angle within  $\text{NH}_3$  does not change significantly when the molecule attaches to  $\text{MX}$  to form either  $\text{H}_3\text{N}\cdots\text{CuX}$  or  $\text{H}_3\text{N}\cdots\text{AgX}$ .

Trends in the  $\text{OC}\cdots\text{CuX}$  and  $\text{H}_3\text{N}\cdots\text{CuX}$  series can also be examined from the perspective of the measured nuclear quadrupole coupling constants. Changes in  $\chi_{aa}$  for the metal and halogen atoms provide insight into the extent of electric charge redistribution when a complex forms from its component units. The measured  $\chi_{aa}$  of  $\text{OC}\cdots\text{CuX}$  and  $\text{H}_3\text{N}\cdots\text{CuX}$  are compared with those for isolated  $\text{MX}$  species and for selected hydrogen- and halogen-bonded complexes in Table 5. The fractional changes in  $\chi_{aa}(\text{M})$  and  $\chi_{aa}(\text{X})$  on formation of the complex from the isolated sub-units,  $\text{B}$  and  $\text{MX}$ , are greater for  $\text{OC}\cdots\text{CuX}$  than for  $\text{H}_3\text{N}\cdots\text{CuX}$  or  $\text{Ar}\cdots\text{CuX}$ . The opposite trend is observed for the hydrogen-bonded complexes,  $\text{OC}\cdots\text{HX}$  and  $\text{H}_3\text{N}\cdots\text{HX}$ . The described differences between the  $\text{B}\cdots\text{MX}$ ,  $\text{B}\cdots\text{HX}^{23}$  and  $\text{B}\cdots\text{XY}^{24}$  series arise because the properties of hydrogen- and halogen-bonded complexes are governed mainly by electrostatic interactions whereas the binding between  $\text{OC}$  or  $\text{NH}_3$  and  $\text{CuX}$  has a significant covalent component. It has been shown that the ionicity of the  $\text{Cu}-\text{X}$  bond of  $\text{OC}\cdots\text{CuX}$  decreases with increasing mass of the halogen atom. An ionicity of 0.73 is determined for  $\text{H}_3\text{N}\cdots\text{CuI}$  during the present work. This is lower than the ionicity of 0.79 determined for  $\text{H}_3\text{N}\cdots\text{CuCl}$  and therefore consistent with the trend identified earlier for the  $\text{OC}\cdots\text{CuX}$  series.

**Table 5.**  $\chi_{aa}({}^{63}\text{Cu})$ ,  $\chi_{aa}(\text{X})$ ,  $r_0(\text{Cu-N/O})$  and  $\Delta r$  for  $\text{OC}\cdots\text{CuX}$ ,  $\text{H}_3\text{N}\cdots\text{CuX}$  and  $\text{CuX}$ .

|      | $\text{H}_3\text{N}\cdots\text{MX}$ |                                | $\text{OC}\cdots\text{MX}$      |                                | $\text{MX}^{\text{a}}$         |                                |
|------|-------------------------------------|--------------------------------|---------------------------------|--------------------------------|--------------------------------|--------------------------------|
|      | $\chi_{aa}(\text{M})$<br>/ MHz      | $\chi_{aa}(\text{X})$<br>/ MHz | $\chi_{aa}(\text{M})$<br>/ MHz  | $\chi_{aa}(\text{X})$<br>/ MHz | $\chi_{aa}(\text{M})$<br>/ MHz | $\chi_{aa}(\text{X})$<br>/ MHz |
| CuF  | 66.196(12)                          | -                              | 75.406(19)                      | -                              | 21.956                         | -                              |
| CuCl | 66.629(24)                          | -23.041(34)                    | 70.8323(210)                    | -21.4735(22)                   | 16.169                         | -32.127                        |
| CuBr | -                                   | -                              | 67.534(12)                      | 171.600(18)                    | 12.851                         | 261.180                        |
| CuI  | 62.943(95)                          | -613.99(28)                    | 64.504(3)                       | -593.465(9)                    | 7.9013(10)                     | -938.3774(8)                   |
| HCl  | -                                   | -47.607(9) <sup>b</sup>        | -                               | -52.086(9) <sup>b</sup>        | -                              | -67.6189(5)                    |
| HI   | -                                   | -1324.891(8) <sup>b</sup>      | -                               | -1346.238(18) <sup>b</sup>     | -                              | -1828.286(9)                   |
| ICl  | -3073.118(6) <sup>b</sup>           | -68.927(3) <sup>b</sup>        | -2953.798(10) <sup>b</sup>      | -79.837(6) <sup>b</sup>        | -2927.859 (2)                  | -85.887(3)                     |
| BrCl | 915.55(2) <sup>b</sup>              | -86.05(1) <sup>b</sup>         | 875.835(5) <sup>b</sup>         | -97.615(3) <sup>b</sup>        | 875.309(1)                     | -102.450(2)                    |
|      | $r_0(\text{Cu-N/O})/\text{\AA}$     | $\Delta r/\text{\AA}$          | $r_0(\text{Cu-N/O})/\text{\AA}$ | $\Delta r/\text{\AA}$          |                                |                                |
| CuF  | 1.89282(63)                         | -0.0071(6) <sup>c</sup>        | 1.7639(4)                       | -0.0198(3) <sup>c</sup>        |                                |                                |
| CuCl | 1.9183(16)                          | 0.0073(7)                      | 1.796(1)                        | 0.0017(7)                      |                                |                                |
| CuBr | -                                   | -                              | 1.8022(9)                       | 0.006(4)                       |                                |                                |
| CuI  | 1.9357(13)                          | 0.0147(5)                      | 1.8154(9)                       | 0.0157(4)                      |                                |                                |

<sup>a</sup> Refs 44, 55, 56, 61-64<sup>b</sup> Ref. 24 and references therein<sup>c</sup>  $\Delta r$  denotes the change in  $r(\text{Cu-X})$  when  $\text{B}\cdots\text{MX}$  form from isolated B and MX units.

### Acknowledgments

The authors thank the EPSRC and the School of Chemistry at Newcastle University for the award of a DTA postgraduate studentship to D.M.B., the European Research Council for the postdoctoral fellowships awarded to S.L.S. and D.P.Z., and for project funding (Grant No. CPFTMW-307000). D.P.Z. also thanks Newcastle University for a SAgE Research Fellowship. A.C.L. thanks the University of Bristol for a Senior Research Fellowship and Newcastle University for a Visiting Professor award. D.P.T. is pleased to acknowledge the Royal Society for the award of a University Research Fellowship. We are also grateful to the EPSRC UK National Service for Computational Chemistry Software (NSCCS) at Imperial College London.

## REFERENCES

1. N. R. Walker and M. C. L. Gerry, *Inorg. Chem.*, 2001, 40, 6158-6166.
2. D. J. Frohman, G. S. Grubbs, Z. Yu and S. E. Novick, *Inorg. Chem.*, 2013, 52, 816-822.
3. G. S. Grubbs, D. A. Obenchain, H. M. Pickett and S. E. Novick, *J. Chem. Phys.*, 2014, 141, 114306.
4. S. G. Francis, S. L. Matthews, O. K. Poleshchuk, N. R. Walker and A. C. Legon, *Angew. Chem. Int. Ed.*, 2006, 45, 6341-6343.
5. N. R. Walker and M. C. L. Gerry, *Inorg. Chem.*, 2002, 41, 1236-1244.
6. C. J. Evans, L. M. Reynard and M. C. L. Gerry, *Inorg. Chem.*, 2001, 40, 6123-6131.
7. V. A. Mikhailov, F. J. Roberts, S. L. Stephens, S. J. Harris, D. P. Tew, J. N. Harvey, N. R. Walker and A. C. Legon, *J. Chem. Phys.*, 2011, 134, 134305.
8. N. R. Walker, D. P. Tew, S. J. Harris, D. E. Wheatley and A. C. Legon, *J. Chem. Phys.*, 2011, 135, 014307.
9. V. A. Mikhailov, D. P. Tew, N. R. Walker and A. C. Legon, *Chem. Phys. Lett.*, 2010, 499, 16-20.
10. D. M. Bittner, D. P. Zaleski, S. L. Stephens, D. P. Tew, N. R. Walker and A. C. Legon, *J. Chem. Phys.*, 2015, 142, 144302.
11. S. L. Stephens, W. Mizukami, D. P. Tew, N. R. Walker and A. C. Legon, *J. Chem. Phys.*, 2012, 137, 174302.
12. D. P. Zaleski, S. L. Stephens, D. P. Tew, D. M. Bittner, N. R. Walker and A. C. Legon, *Phys. Chem. Chem. Phys.*, 2015, 17, 19230-19237.
13. S. L. Stephens, D. M. Bittner, V. A. Mikhailov, W. Mizukami, D. P. Tew, N. R. Walker and A. C. Legon, *Inorg. Chem.*, 2014, 53, 10722-10730.
14. S. L. Stephens, D. P. Tew, V. A. Mikhailov, N. R. Walker and A. C. Legon, *J. Chem. Phys.*, 2011, 135, 024315.
15. D. P. Zaleski, J. C. Mullaney, D. M. Bittner, D. P. Tew, N. R. Walker and A. C. Legon, *J. Chem. Phys.*, 2015, 143, 164314.
16. Q. Wang, B. Zhang and Z. Huang, *Chem. Phys. Lett.*, 2014, 614, 5-9.
17. G. Zhang, H. Yue, F. Weinhold, H. Wang, H. Li and D. Chen, *ChemPhysChem*, 2015, 16, 2424-2431.
18. G. Zhang, X. Zhao and D. Chen, *J. Phys. Chem. A*, 2013, 117, 10944-10950.
19. H. Li, Q. Li, R. Li, W. Li and J. Cheng, *J. Chem. Phys.*, 2011, 135, 074304.
20. G. Margraf, J. W. Bats, M. Bolte, H.-W. Lerner and M. Wagner, *Chem. Commun.*, 2003, 8, 956-957.
21. P. Woidy, A. J. Karttunen, M. Widenmeyer, R. Niewa and F. Kraus, *Chem. Eur. J.*, 2015, 21, 3290-3303.
22. S. G. Batten and A. C. Legon, *Chem. Phys. Lett.*, 2006, 422, 192-197.
23. A. C. Legon and D. J. Millen, *Faraday Discuss. Chem. Soc.*, 1982, 73, 71-87.
24. A. C. Legon, *Angew. Chem. Int. Ed.*, 1999, 38, 2686-2714.

25. S. L. Stephens, W. Mizukami, D. P. Tew, N. R. Walker and A. C. Legon, *J. Chem. Phys.*, 2012, 136, 064306.
26. D. P. Zaleski, S. L. Stephens and N. R. Walker, *Phys. Chem. Chem. Phys.*, 2014, 16, 25221-25228.
27. H. J. Werner, P. J. Knowles, G. Knizia, F. R. Manby, M. Schütz, , *WIREs Comput Mol Sci*, 2012, 2, 242-253, doi: 10.1002/wcms.82
28. C. Hättig, D. P. Tew and A. Köhn, *J. Chem. Phys.*, 2010, 132, 231102.
29. C. Hättig, W. Klopper, A. Köhn and D. P. Tew, *Chem. Rev.*, 2012, 112, 4-74.
30. K. Raghavachari, G. W. Trucks, J. A. Pople and M. Head-Gordon, *Chem. Phys. Lett.*, 1989, 157, 479-483.
31. A. K. Peterson and C. Puzzarini, *Theor. Chem. Acc.*, 2005, 114, 283-296.
32. M. Dolg, U. Wedig, H. Stoll and H. Preuss, *J. Chem. Phys.*, 1987, 86, 866-872.
33. K. A. Peterson, D. Figgen, E. Goll, H. Stoll and M. Dolg, *J. Chem. Phys.*, 2003, 119, 11113-11123.
34. I. S. Lim, P. Schwerdtfeger, B. Metz and H. Stoll, *J. Chem. Phys.*, 2005, 122, 104103.
35. C. Hättig, *Phys. Chem. Chem. Phys.*, 2005, 7, 59-66.
36. F. Weigend, *J. Comput. Chem.*, 2008, 29, 167-175.
37. E. F. Valeev, *Chem. Phys. Lett.*, 2004, 395, 190-195.
38. A. Hellweg, C. Hättig, S. Höfener and W. Klopper, *Theor. Chem. Acc.*, 2007, 117, 587-597.
39. M. J. Frisch, G. W. Trucks, H. B. Schlegel, G. E. Scuseria, M. A. Robb, J. R. Cheeseman, G. Scalmani, V. Barone, B. Mennucci, G. A. Petersson, H. Nakatsuji, M. Caricato, X. Li, H. P. Hratchian, A. F. Izmaylov, J. Bloino, G. Zheng, J. L. Sonnenberg, M. Hada, M. Ehara, K. Toyota, R. Fukuda, J. Hasegawa, M. Ishida, T. Nakajima, Y. Honda, O. Kitao, H. Nakai, T. Vreven, J. A. Montgomery Jr., J. E. Peralta, F. Ogliaro, M. Bearpark, J. J. Heyd, E. Brothers, K. N. Kudin, V. N. Staroverov, T. Keith, R. Kobayashi, J. Normand, K. Raghavachari, A. Rendell, J. C. Burant, S. S. Iyengar, J. Tomasi, M. Cossi, N. Rega, J. M. Millam, M. Klene, J. E. Knox, J. B. Cross, V. Bakken, C. Adamo, J. Jaramillo, R. Gomperts, R. E. Stratmann, O. Yazyev, A. J. Austin, R. Cammi, C. Pomelli, J. W. Ochterski, R. L. Martin, K. Morokuma, V. G. Zakrzewski, G. A. Voth, P. Salvador, J. J. Dannenberg, S. Dapprich, A. D. Daniels, O. Farkas, J. B. Foresman, J. V. Ortiz, J. Cioslowski and D. J. Fox, Gaussian 09, Revision D.01, Gaussian, Inc., Wallingford CT, 2009.
40. S. L. Stephens and N. R. Walker, *J. Mol. Spectrosc.*, 2010, 263, 27-33.
41. D. D. Nelson, G. T. Fraser, K. I. Peterson, K. Zhao, W. Klemperer, F. J. Lovas and R. D. Suenram, *J. Chem. Phys.*, 1986, 85, 5512-5518.
42. S. L. Stephens, N. R. Walker and A. C. Legon, *Phys. Chem. Chem. Phys.*, 2011, 13, 20736-20744.
43. H. S. P. Müller and M. C. L. Gerry, *J. Chem. Phys.*, 1995, 103, 577-583.
44. S. G. Batten, A. G. Ward and A. C. Legon, *J. Mol. Struct.*, 2006, 780-781, 300-305.
45. D. M. Bittner, D. P. Zaleski, S. L. Stephens, N. R. Walker and A. C. Legon, *ChemPhysChem*, 2015, 16, 2630-2634.
46. D. D. Nelson, G. T. Fraser and W. Klemperer, *J. Chem. Phys.*, 1985, 83, 6201-6208.
47. PGOPHER, a Program for Simulating Rotational, Vibrational and Electronic Structure, C. M. Western, University of Bristol, <http://pgopher.chm.bris.ac.uk>.
48. Z. Kisiel, *J. Mol. Spectrosc.*, 2003, 218, 58-67.
49. C. C. Costain, *J. Chem. Phys.*, 1958, 29, 864-874.
50. A. Chutjian, *J. Mol. Spectrosc.*, 1964, 14, 361-370.
51. C. Costain, *Trans. Am. Crystallogr. Assoc.*, 1966, 2, 157-164.
52. J. Kraitchman, *Am. J. Phys.*, 1953, 21, 17-24.
53. J. K. G. Watson, A. Roytburg and W. Ulrich, *J. Mol. Spectrosc.*, 1999, 196, 102-119.
54. D. M. Bittner, N. R. Walker and A. C. Legon, *J. Chem. Phys.*, 2016, 144, 074308.
55. R. J. Low, T. D. Varberg, J. P. Connelly, A. R. Auty, B. J. Howard and J. M. Brown, *J. Mol. Spectrosc.*, 1993, 161, 499-510.

56. J. Hoefft, F. J. Lovas, E. Tiemann and T. Törring, *Z. Naturforsch. A Phys. Sci.*, 1970, 25, 35-39.
57. C. H. Townes and B. P. Dailey, *J. Chem. Phys.*, 1949, 17, 782-796.
58. B. P. Dailey and C. H. Townes, *J. Chem. Phys.*, 1955, 23, 118-123.
59. W. Gordy and R. L. Cook, *Microwave Molecular Spectra*, Wiley, New York, 1984.
60. C. J. Evans and M. C. L. Gerry, *J. Chem. Phys.*, 2000, 112, 9363-9374.
61. F. H. de Leluw and A. Dymanus, *J. Mol. Spectrosc.*, 1973, 48, 427-445.
62. E. Herbst and W. Steinmetz, *The J. Chem. Phys.*, 1972, 56, 5342-5346.
63. R. E. Willis and W. W. Clark, *J. Chem. Phys.*, 1980, 72, 4946-4950.
64. F. A. Van Dijk and A. Dymanus, *Chem. Phys. Lett.*, 1968, 2, 235-236.